



# Structural and shielding effectiveness properties of (NiFe<sub>2</sub>O<sub>4</sub>/chopped strands) composites for 6.5–18 GHz applications

Ethem İlhan Sahin<sup>1</sup>, Jamal-Eldin F. M. Ibrahim<sup>2,\*</sup>, Mehriban Emek<sup>3</sup>, Bahaddin Sinsoyal<sup>4</sup>, and Alina Amanzholova<sup>5</sup>

<sup>1</sup> Advanced Technology Research and Application Center, Adana Alparslan Türkeş Science and Technology University, Adana, Turkey

<sup>2</sup> Corresponding Author, Doctoral School of Material Science and Technology, Institute of Ceramic and Polymer Engineering, Faculty of Material Science and Engineering, University of Miskolc, Miskolc, Hungary

<sup>3</sup> Department of Physics, Golbasi Vocational School, Computer Technologies, Adiyaman University, Gölbaşı, Adiyaman 02040, Turkey

<sup>4</sup> Department of Mathematics and Computer Engineering, Faculty of Engineering, İstanbul Gedik University, Kartal, İstanbul 34876, Turkey

<sup>5</sup> Department of Mathematics, Faculty of Science, Khoja Akhmet Yassawi International Kazakh-Turkish University, Turkistan, Kazakhstan

**Received:** 22 April 2024

**Accepted:** 9 June 2024

**Published online:**  
16 July 2024

© The Author(s), 2024

## ABSTRACT

In this research, a mixed oxide technique was employed to create composite materials comprising NiFe<sub>2</sub>O<sub>4</sub>-chopped strands, aimed at evaluating their structural properties and microwave shielding effectiveness. The composites, produced through a hot-pressing process with varying proportions of NiFe<sub>2</sub>O<sub>4</sub> and chopped strands, were integrated with epoxy to enhance their shielding capabilities. X-ray diffraction confirmed the formation of single-phase NiFe<sub>2</sub>O<sub>4</sub>, free from secondary phases. Scanning electron microscopy analysis corroborated the presence of cubic crystalline NiFe<sub>2</sub>O<sub>4</sub>, without microstructural impurities. The microwave shielding performance of the composites was assessed within the 6.5–18 GHz frequency range using a network analyzer (NA), revealing a minimum shielding effectiveness of –36.34 dB at 16.56 GHz for a 1.3 mm thick sample. These findings demonstrate the successful fabrication of NiFe<sub>2</sub>O<sub>4</sub>-chopped strands composites with tunable microwave shielding properties, achieved by adjusting the NiFe<sub>2</sub>O<sub>4</sub> content, allowing for tailored performance across various frequency bands.

Address correspondence to E-mail: jamalfadoul@gmail.com

E-mail Addresses: shnethem@gmail.com; memek@adiyaman.edu.tr; alina.amanzhol07@gmail.com

<https://doi.org/10.1007/s10854-024-12965-y>

## 1 Introduction

As the prevalence of electronic gadgets and satellite communication networks relying on wireless technology continues to rise, the need for high-frequency applications has seen a corresponding increase. With the extensive utilization of electromagnetic waves in communication systems, there comes the unintended consequence of generating a significant quantity of undesirable electromagnetic waves. This phenomenon, characterized by the detrimental proliferation of electromagnetic pollution, is commonly referred to as electromagnetic interference (EMI) [1]. Electromagnetic radiation can also have a negative impact on various aspects of daily life, including the sensitivity and functionality of many electrical equipment [2]. In the environment we live in, we are constantly under a network of wireless microwave signals that we cannot see, which harms us. Exposure to silent and unseen high-intensity electromagnetic waves can lead to a range of health issues and detrimental effects, primarily manifesting through physiological alterations [3–5].

The GHz frequency range is extensively employed in communication systems and various electronic devices. The abundant electromagnetic radiation stemming from the rapid advancement and downsizing of electronic technologies, such as wireless communication, GPS, and mobile devices, is now recognized as an additional source of environmental contamination [6]. This pervasive electromagnetic pollution poses significant risks to both human health and the well-being of our environment [7, 8].

There are several control strategies to prevent and reduce electromagnetic wave exposure such as using engineering techniques, use of personal protective equipment, limiting exposure time, and reducing exposure levels to acceptable levels [9]. To protect systems and people from this electromagnetic pollution, it is necessary to use shielding materials against EMI [10].

EMI shielding materials offer defense against electromagnetic waves through mechanisms designed to either absorb or reflect unwanted EM waves [11]. It's worth noting that, from an environmental perspective, the absorption mechanism is favored over reflection [12, 13]. EMI shielding is influenced by multiple factors, with reflection loss being one of them. This aspect hinges on the interaction between mobile charge carriers (electrons or holes) and incoming EM waves. Another influential factor is absorption loss,

which is determined by how magnetic and electrical dipoles interact with EM waves. The third mechanism, referred to as the multiple reflection effect, comes into play when there are extensive and sizable surface or interfacial regions within the shielding material, leading to internal reflections [14].

EMI shielding uses composite materials with non-continuous conductive additives like metallic wires, particles, metal flakes, and carbon fibers [15, 16]. Polymer matrix composites are favored for their versatility and ability to address material shortcomings.  $\text{NiFe}_2\text{O}_4$  spinel ferrites are important for their magnetic properties, including superparamagnetic behavior, making them useful in various high-frequency applications [17]. These ferrites exhibit high saturation magnetization, acid resistance, and thermal stability, which are beneficial for microwave absorption [18, 19]. Their properties depend on factors like chemical composition, microstructure, and doping parameters. While  $\text{NiFe}_2\text{O}_4$  has excellent absorption properties, its high density and conductivity can be limiting. Therefore, combining ferrite powder with non-magnetic polymers enhances performance, making ferrite/polymer composites ideal for lightweight and flexible microwave absorbers [20, 21].

Glass fibers (chopped strands or glass fiber roving) are among the most important reinforcements within the high-performance composite manufacturing industry. It also has outstanding mechanical properties [22]. Chopped wires are corrosion-resistant, light, elastic and inexpensive and serve as reinforcement for the composite material. It is also used for multiple purposes due to its excellent strength, moisture resistance and electrical and fire insulation. The qualities of the composite are determined by the interface connection between the glass fibers and the matrix resin [23].

Previous literature on the development and testing of materials for electromagnetic shielding has demonstrated significant advancements in this field. Kumar et al. [24] investigated  $\text{NiFe}_2\text{O}_4/\text{rGO}$  nanocomposite, which showed a total shielding effectiveness (SET) of 38.2 dB at 10.8 GHz with a thickness of 2 mm. This high SET is attributed to the nanocomposite's superior dielectric and magnetic loss properties, enhanced absorption, and multiple reflections. Caramitu et al. [25] explored polymer composite materials incorporating ferrite nano-powder, revealing that these composites are effective in both lower frequencies and the microwave domain while also exhibiting high thermal stability. Radoń et al. [26] focused on

(Zn,Mg,Ni,Fe,Cd)Fe<sub>2</sub>O<sub>4</sub> high entropy ferrite powder, which displayed excellent microwave absorption properties with reflection loss (RL) below -25 dB and shielding effectiveness (SE) below -50 dB in the 1.9 to 2.1 GHz range for layers 0.8–1 cm thick. Shakir et al. [27] examined the EMI shielding properties of polystyrene/polyaniline blends with nickel spinel ferrites, noting a significant enhancement in shielding from -3 dB to less than -35 dB across a broad frequency range of 0.1 to 20 GHz. Heryanto et al. [28] synthesized CoFeO<sub>3</sub> using simple mechanical alloying to enhance multiple reflections and scattering, thereby improving EMI wave absorption. They observed a reflection loss of -55 dB at 10–11 GHz with an 8 mm thick sample, demonstrating CoFeO<sub>3</sub>'s significant potential as a composite material for microwave absorption applications [28]. These studies collectively highlight the diverse approaches and material innovations being pursued to achieve effective EMI shielding across various frequency ranges and material properties.

In the present study, a new NiFe<sub>2</sub>O<sub>4</sub>-chopped strands composite was developed for the first time, employing optimal parameters, and its shielding efficiency properties were evaluated. These new composites were fabricated by blending different quantities of components with epoxy powder, and NiFe<sub>2</sub>O<sub>4</sub>-chopped strands composites were fashioned at various ratios, each with a thickness of 1.3 mm, using a hot pressing technique. Phase identification within the composites was conducted using an X-ray diffraction (XRD) device [29, 30], while the morphology of the structures was analyzed via scanning electron microscopy (SEM) measurements. The chemical compositions were determined using an Oxford-Inca 7274 instrument in conjunction with a dispersive spectrometer (EDS). The microwave shielding efficiency of the NiFe<sub>2</sub>O<sub>4</sub>-chopped strand composites was assessed across a wide frequency range (6.5–18 GHz) using a network analyzer.

## 2 Experimental

### 2.1 Preparation of NiFe<sub>2</sub>O<sub>4</sub>

The synthesis of NiFe<sub>2</sub>O<sub>4</sub> powder was carried out using a solid-state reaction route. Stoichiometric amounts of high-purity nickel oxide (NiO, 97% purity from Acrosorganics) and hematite (Fe<sub>2</sub>O<sub>3</sub>, 99% purity from Sigma-Aldrich) were selected as

the starting reactants. Specifically, 6.4 g of NiO and 14.2 g of Fe<sub>2</sub>O<sub>3</sub> were measured for the synthesis. The measured amounts of NiO and Fe<sub>2</sub>O<sub>3</sub> powders were placed in a beaker. To facilitate the formation of a homogeneous mixture, absolute ethanol was added to the beaker. The mixture was thoroughly stirred to ensure uniform distribution of the reactants. The homogeneous mixture was then transferred to a ball mill. Zirconium balls were used as the milling medium. The milling process was carried out for 20 h, ensuring thorough mixing and reduction in particle size. After milling, the resulting slurry was dried in an oven at 100 °C for 20 h. This step was crucial to remove the ethanol and prepare the dry reactant mixture for the subsequent calcination step. The dried mixture was placed in a sealed alumina crucible and subjected to calcination. The calcination was performed at 600 °C for 4 h. This step facilitated the initial solid-state reaction between NiO and Fe<sub>2</sub>O<sub>3</sub> to form NiFe<sub>2</sub>O<sub>4</sub>. Post-calcination, the resulting powder was ground using an agate mortar to ensure fine and uniform particle size. The ground NiFe<sub>2</sub>O<sub>4</sub> powder was then sintered at temperatures ranging between 1100 °C and 1300 °C for 4 h. The heating and cooling rates were maintained at 300 °C/h. This final step ensured the formation of single-phase NiFe<sub>2</sub>O<sub>4</sub> powders with the desired crystalline structure. By following these steps, high-purity NiFe<sub>2</sub>O<sub>4</sub> powder was successfully synthesized, suitable for various applications requiring precise material properties.

### 2.2 Preparation of NiFe<sub>2</sub>O<sub>4</sub>/chopped strands composites

The chopped strands were first crushed and pulverized in a durable agate mortar and then mixed with sintered NiFe<sub>2</sub>O<sub>4</sub> powders in stoichiometric ratios. The mixtures were prepared in plastic containers with adjusted weight ratios of 80–20% and 60–40% (NiFe<sub>2</sub>O<sub>4</sub> to chopped strands). These compositions were homogenized by placing them in sealed plastic containers with zirconia balls and ethanol and then rotating them in a mill for 20 h. Following the milling process, the separate slurries were dried in an oven at 100 °C for 24 h. Each dried mixture was then washed with ethanol by filtration, and the washed slurry samples were subjected to a vacuum at 60 °C for 24 h. This process resulted in the production of NiFe<sub>2</sub>O<sub>4</sub>/chopped strand composites with weight ratios of 80–20% and 60–40%.

### 2.3 Preparation of epoxy- (NiFe<sub>2</sub>O<sub>4</sub>/chopped strands) composites

The NiFe<sub>2</sub>O<sub>4</sub>/chopped strands compound powders were combined with epoxy powder to form composite materials, maintaining a weight ratio of 5:1 in grams for the mixed powders to epoxy. The resulting mixture was shaped into pellets using a temperature-controlled hydraulic press, applying a consistent pressure of 5 MPa at 100 °C for 1 h (Fig. 1). These pellets, with a thickness of 1.3 mm, were designed specifically for shielding effectiveness assessments. The novel NiFe<sub>2</sub>O<sub>4</sub>/chopped strands composites, crafted with epoxy, were engineered to provide low shielding effectiveness across a wide frequency range of 6.5 to 18 GHz.

### 2.4 Characterization methods

The phases identification of the samples were characterized using X-ray diffraction (XRD) with Cu-K $\alpha$  radiation ( $\lambda = 1.5406 \text{ \AA}$ ) over a range of  $2\theta$ : 10–70°,

at a scanning speed of 1°/min. Furthermore, the microstructure and morphology of the samples were examined utilizing a JEOL 5910LV scanning electron microscope (SEM) in the secondary electron mode. To facilitate detailed elemental analysis, this SEM was coupled with an advanced EDAX Genesis energy-dispersive X-ray analyzer (EDX). Before conducting the analysis, the samples were coated with a thin layer of gold using a specialized coating spray device to improve their reflective properties and ensure high-quality imaging. Magnetic hysteresis measurements are conducted using a Cryogenic Limited Physical Properties Measurement System (PPMS) equipped with a Vibrating Sample Magnetometer (VSM). Finally, the microwave shielding efficiency of the novel NiFe<sub>2</sub>O<sub>4</sub> composites was assessed across the 6.5–18 GHz frequency spectrum, utilizing a N 5230A PNA series network analyzer device.

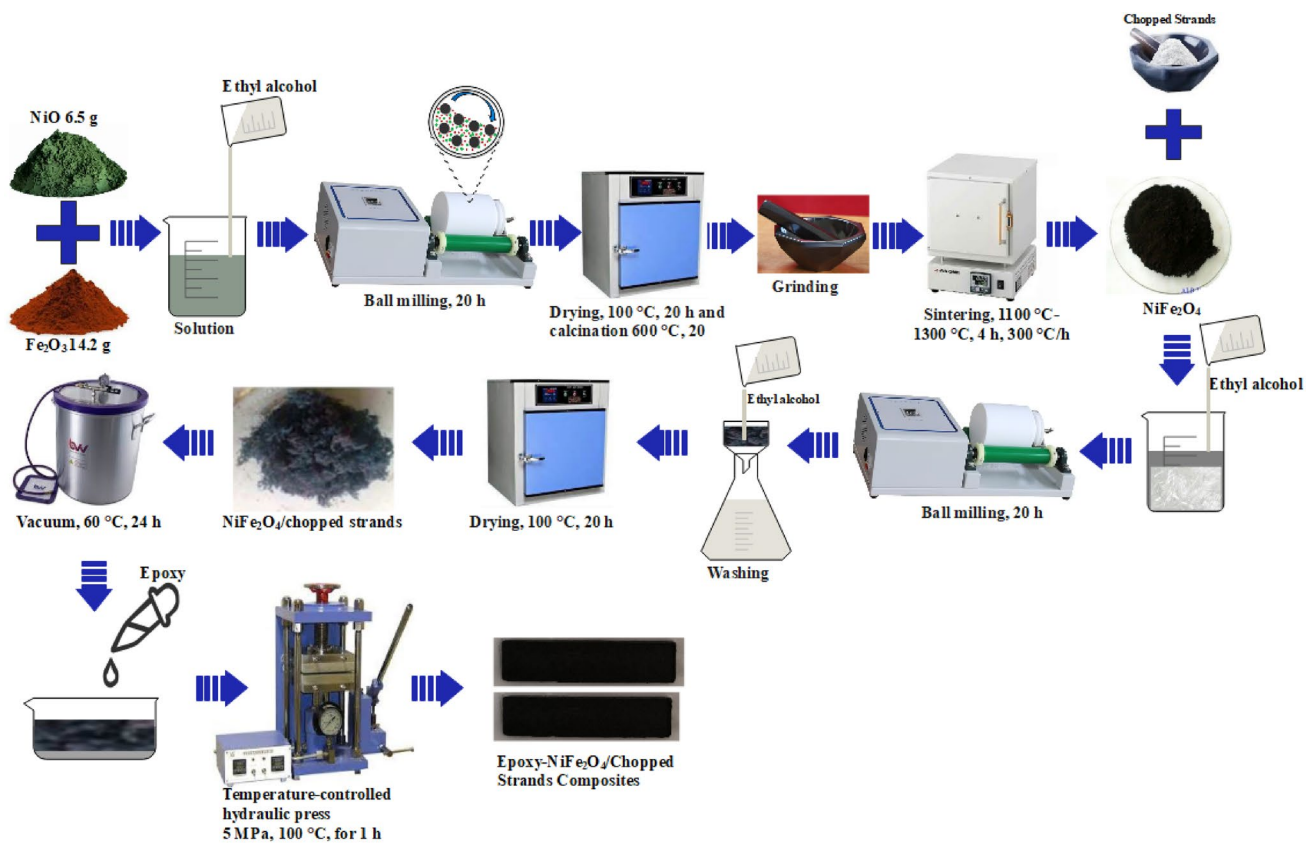


**Fig. 1** Illustration of the synthesis method of epoxy-NiFe<sub>2</sub>O<sub>4</sub>/chopped strands composites

### 3 Results and discussion

#### 3.1 XRD investigations of NiFe<sub>2</sub>O<sub>4</sub>/ chopped strands

To analyze the structure of NiFe<sub>2</sub>O<sub>4</sub>, X-ray diffraction (XRD) spectroscopy was conducted. NiFe<sub>2</sub>O<sub>4</sub> underwent sintering at 1200 °C for a duration of 4 h. The XRD examination revealed the formation of singular-phase structures of NiFe<sub>2</sub>O<sub>4</sub> (as depicted in Fig. 2).

The X-ray diffraction (XRD) patterns for NiFe<sub>2</sub>O<sub>4</sub> and Chopped strands (Fig. 2) clearly illustrate the predominant phases present, namely NiFe<sub>2</sub>O<sub>4</sub>. The NiFe<sub>2</sub>O<sub>4</sub> diffraction planes (111), (220), (311), (222), (400), (422), (511), (440), and were observed at 2θ diffraction angles of 18.3°, 30.2°, 35.6°, 37.2°, 43.3°, 53.8°, 57.3° and 62.9°, respectively. These results were indexed using PDF Card No. 44–1485, confirming a cubic phase with a space group of Fd-3 m. The crystallite size of the synthesized NiFe<sub>2</sub>O<sub>4</sub> is determined using Scherrer's formula. For a large crystal containing minor dislocations, the Scherrer equation can be expressed as follows [31]:

$$D = 0.94\lambda / \beta \cos \theta \quad (1)$$

In this equation, *D* represents the average crystallite size,  $\lambda$  is the wavelength of the Cu K $\alpha$  radiation,  $\beta$  is the

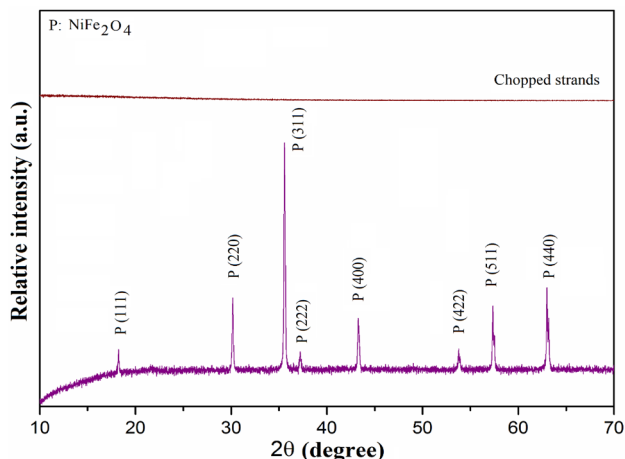


**Fig. 2** XRD pattern for NiFe<sub>2</sub>O<sub>4</sub> (single-phase sintered at 1200 °C for 4 h, respectively) and Polyaniline

full width at half-maximum (FWHM) of the diffraction peak, and  $\theta$  is the Bragg diffraction angle. Utilizing this formula, the average crystallite size is estimated to be approximately 33.2 nm (Table 1).

The high peak intensity is indicative of increased crystallinity, reflecting the degree of structural regularity within the solid. This heightened crystallinity significantly impacts both the hardness and density of the material [32]. This analysis demonstrates that through the method of oxide mixture and subsequent sintering at the appropriate calcination temperature, a single-phase structure for NiFe<sub>2</sub>O<sub>4</sub> with a homogeneous phase composition was successfully achieved, eliminating any potential intermediate phases during the process. The absence of secondary phases in sintered NiFe<sub>2</sub>O<sub>4</sub> was confirmed by XRD analysis.

Experimental lattice parameters and unit cell volume were meticulously calculated using FullProf, as detailed in Table 1. The obtained XRD model was accurately matched with the standard XRD model of NiFe<sub>2</sub>O<sub>4</sub>, confirming the structural consistency of the synthesized material.

#### 3.2 SEM analysis of NiFe<sub>2</sub>O<sub>4</sub>

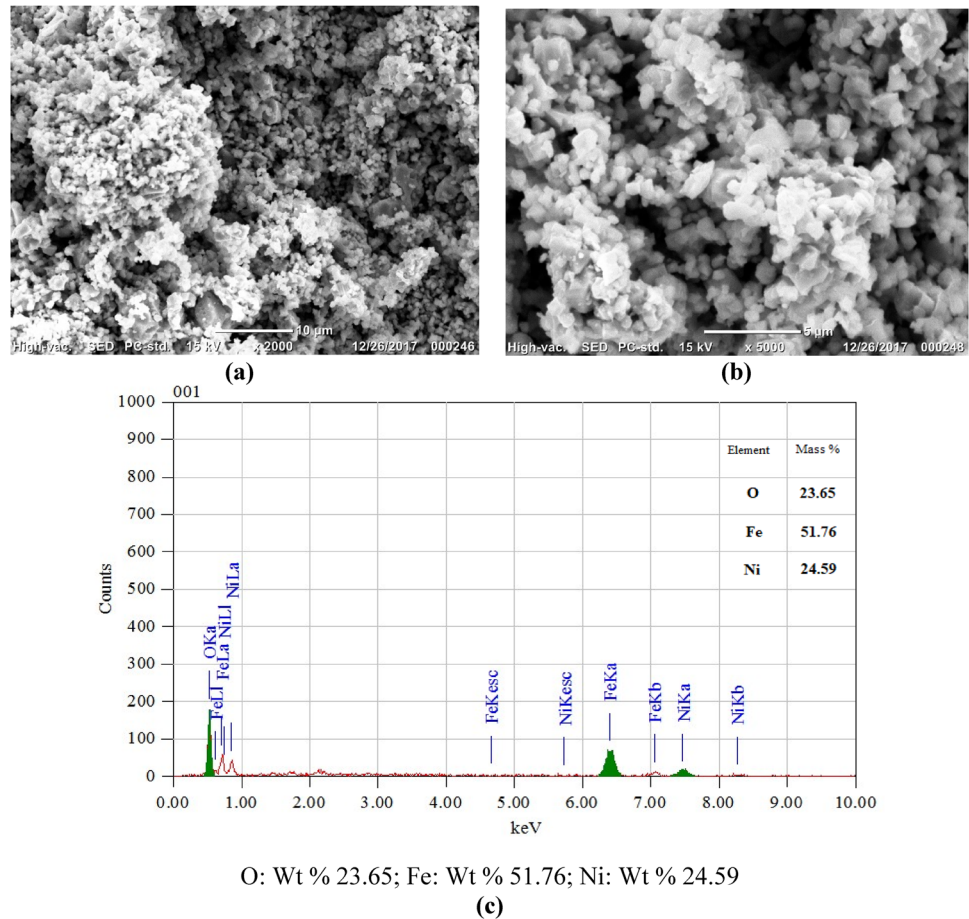
To delve into the microstructures and morphology of the NiFe<sub>2</sub>O<sub>4</sub> samples sintered at 1200 °C for 4 h, we conducted scanning electron microscope (SEM) analysis. Mirroring the findings of the XRD analysis, the SEM examination revealed the presence of solely cubic crystalline NiFe<sub>2</sub>O<sub>4</sub> in the samples. There were no indications of secondary phases or microstructural impurities, as depicted in Fig. 3a, b. It's worth noting that NiFe<sub>2</sub>O<sub>4</sub> possesses a centrosymmetric cubic crystal structure (Fig. 3).

The microstructure exhibited the formation of grains with morphologies that complemented each other. Electromagnetic shielding is significantly influenced by the multi-reflection effect, which indicates internal reflections within the material. This phenomenon frequently arises in materials with extensive surface areas or interfacial regions. The sintered NiFe<sub>2</sub>O<sub>4</sub>, featuring porous structures, likely possesses substantial specific surface areas and

**Table 1** Using FullProf, computed lattice parameters of a NiFe<sub>2</sub>O<sub>4</sub> specimen (sintered for 4 h at 1200 °C)

Sample	Average Crystallite Size (nm)	a (Å)	b (Å)	c (Å)	Volume (Å <sup>3</sup> )	Space Group	SYS
NiFe <sub>2</sub> O <sub>4</sub>	33.2	8.339	8.339	8.339	579.95	Fd-3 m (227)	Cubic

**Fig. 3** SEM pictures of single phase  $\text{NiFe}_2\text{O}_4$  **a** at  $\times 2000$  **b** at  $\times 5000$  **c** EDS analysis of  $\text{NiFe}_2\text{O}_4$  at  $\times 5000$



multiple internal grain boundaries [33, 34]. These characteristics contribute to an enhancement in the effectiveness of shielding electromagnetic waves.

### 3.3 Magnetic properties of $\text{NiFe}_2\text{O}_4$ / chopped strands compositions

Magnetic hysteresis measurement is performed with the Cryogenic Limited PPMS (Physical Properties Measurement System) integrated Vibrating Sample Magnetometer (VSM) module device. VSM measurement is used to evaluate the magnetic properties of powdered samples within a defined magnetic field range. This characterization is carried out either at room temperature or at a specific temperature value.

Magnetic measurement of  $\text{NiFe}_2\text{O}_4$  samples, obtained by the mixture of oxides method from  $\text{NiO} + \text{Fe}_2\text{O}_3$  composition and sintered at  $1200^\circ\text{C}$ , was carried out at room temperature. The magnetization of  $\text{NiFe}_2\text{O}_4$  samples as a function of the magnetic field (M-H) is shown in Fig. 4. Ferromagnetic behavior was

obtained by measuring the saturation magnetization value of  $45.3\text{ emu/g}$  (Ms) of the pure  $\text{NiFe}_2\text{O}_4$  sample (Fig. 4). Since the Choppes strands sample did not

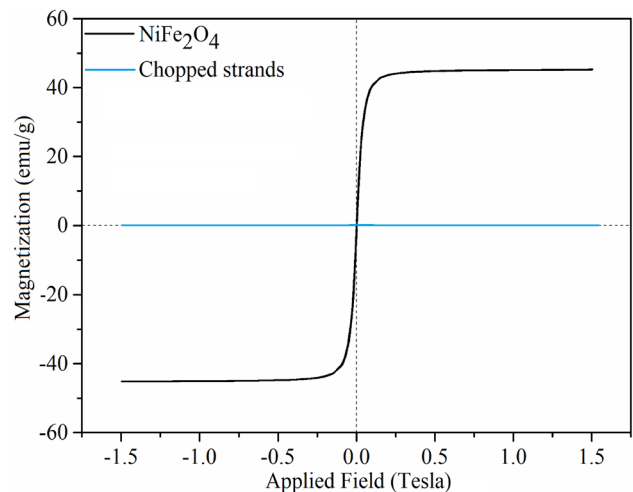


**Fig. 4** Magnetic hysteresis loops, pure  $\text{NiFe}_2\text{O}_4$  heat treated at  $1200^\circ\text{C}$  for 4 h and chopped strands

show magnetic properties as expected, the saturation magnetization value was measured as 0.

### 3.4 Shielding effect measurements of NiFe<sub>2</sub>O<sub>4</sub>/chopped strands

Figure 5 illustrates the frequency-dependent changes in the shielding efficiency values of epoxy-based composites comprising (NiFe<sub>2</sub>O<sub>4</sub>/Chopped strands) within the 6.5–18 GHz frequency spectrum. To ensure accuracy, the measurements were repeated for samples prepared with a consistent thickness of 1.3 mm. Table 2 provides a reference for microwave shielding efficiency values of various materials found in existing

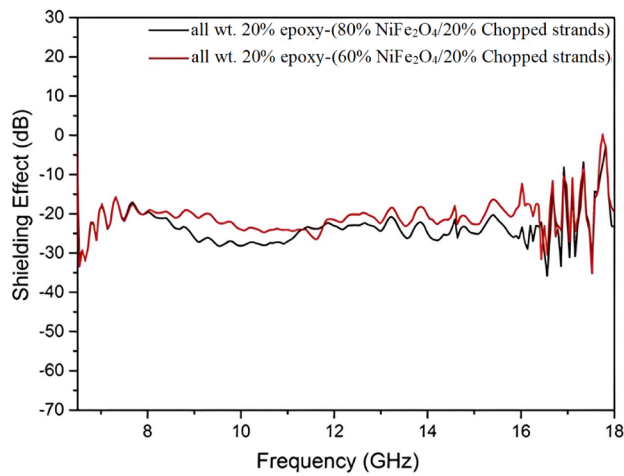


**Fig. 5** Microwave shielding efficiency of epoxy-(NiFe<sub>2</sub>O<sub>4</sub>/Chopped strands) composites: all wt 20% epoxy-(80% NiFe<sub>2</sub>O<sub>4</sub>/20% chopped strands) compositions, all wt. 20% epoxy-(60% NiFe<sub>2</sub>O<sub>4</sub>-40% chopped strands) compositions

literature which showed comparable results to this study.

SE (insertion loss) measurements of the composites were analyzed using an N 5230A PNA series Network Analyzer (Agilent Technologies). The setup consists of a sample holder whose input and output are connected to the network analyzer. To perform the SE test, coaxial holders with sufficient diameters that maintained 50-Ω impedance at the input and output ports were used. The sample was clamped between the two halves of the sample holder. Before proceeding with the measurement, a sample-free value was first measured.

The purpose of any shielding effectiveness (SE) test is to determine and measure the insertion loss resulting from the insertion of a material between the source and the signal analyzer. SE is determined by measuring electric field strength levels with both reference (ER) and load (EL) samples. This is without and with protective material respectively [41]:

$$SE = 20 \log_{10}(E_R/E_L) = (dB)_R - (dB)_L \tag{2}$$

Besides, this can also be determined by measuring power,

$$SE = 10 \log_{10}(P_R/P_L) \tag{3}$$

On the other hand, SE is usually expressed in decibels, (dB) by the following equation [42]:

Where:

$$SE = 10 \log P_1/P_2(dB) \tag{4}$$

$P_1$  = received power with the material present, and  $P_2$  = received power without the material present.

**Table 2** The microwave shielding effect properties of other results in the literature

Sample	Thickness (mm)	Shielding Effectiveness value (dB)	Frequency (GHz)	Reference
Epoxy-NiFe <sub>2</sub> O <sub>4</sub> /chopped strands composite	1.3	-36.34	16.56	This work
High entropy (Zn,Fe,Ni,Mg,Cd) Fe <sub>2</sub> O <sub>4</sub> ferrite	8	-50	1.9 to 2.1	[26]
NiFe <sub>2</sub> O <sub>4</sub> -RGO-polypropylene nanocomposites	2	29.4	5.8 to 8.2	[35]
Polyaniline/ nickel spinal ferrites	0.25	-35	0.1 to 20	[27]
NiFe <sub>1.7</sub> Cu <sub>0.3</sub> O <sub>3.85</sub> /aniline: 1/3	2	-29.74	6.82	[30]
% 25 MWCNT	1.5	-39	1.6	[36]
Chopped strands/Ba(Zn <sub>1/3</sub> Nb <sub>2/3</sub> )O <sub>3</sub> (at 20–80 wt.%)	1.4	-24.96	6.22	[37]
CF-PTh/graphene	7×5	-30	12.4–18	[38]
CF/epoxy-composite	2	-29.4	12.4	[39]
Graphene 2.5 wt%: epoxy	2	-29	8.2–12.4	[40]

If the receiver readout is in units of voltage, the following equation could be used:

$$SE = 20 \log V_1/V_2(\text{dB}) \quad (5)$$

where:  $V_1$  and  $V_2$  = respective voltage levels with and without a material present.

The samples were then placed sequentially into the device and compressed evenly at all different locations, always to ensure consistent pressure throughout the sample. The difference between the presence and absence of samples was displayed on the computer as shielding effectiveness (SE) values. The holder is an enlarged coaxial transmission line with unique tapered sections and matching notches that maintain a characteristic impedance of 50 ohms over the entire length of the holder [42]. The measurement of the device was checked by repeatedly measuring smooth, 1.3 mm thick, and rectangular-shaped samples. Sample thickness is a critical dimension. For the best repeatability of SE measurements, the reference sample area and the thickness of the load sample should be the same.

The measured SE values of composites depend on geometry and orientation. The performance value of the shielding effect depends on how far the incident electromagnetic wave passes through the composite material.

Among the  $\text{NiFe}_2\text{O}_4$ /Chopped strands composites, the shielding effect capabilities of  $\text{NiFe}_2\text{O}_4$ -chopped strands (80–20% by weight) were clearly superior to those of  $\text{NiFe}_2\text{O}_4$ -chopped strands (60–40% by weight). This specific composite yielded the lowest recorded value of -36.34 dB at 16.56 GHz (as shown in Fig. 5). At various frequencies, it provided shielding effect values of - 32.04 dB, - 32.54 dB, - 29.43 dB, and - 35.61 dB for 6.66 GHz, 17.53 GHz, 16.86 GHz, and 16.12 GHz, respectively. Furthermore, it maintained a shielding effect of less than - 10 dB across a wide bandwidth, spanning from 6.5 to 16.88 GHz.

This composite material consistently exhibited shielding effectiveness values below - 20 dB between 6.5 and 6.92 GHz, 8.09 to 15.31 GHz, and 15.48 to 16.61 GHz.

In contrast, the epoxy-based composition of  $\text{NiFe}_2\text{O}_4$  (60–40% by weight) displayed the lowest shielding effectiveness value at - 35.61 dB, occurring at a frequency of 17.51 GHz. It also recorded the second-lowest shielding effectiveness value at - 33.71 dB, observed at 6.54 GHz.

At different frequencies, it recorded shielding effect values of - 31.8 dB, - 26.83 dB, - 23.49 dB, - 32.04 dB, - 30.63 dB, and - 27.3 dB for 6.67 GHz, 11.62 GHz, 13.52 GHz, 16.44 GHz, 16.56 GHz, and 17.05 GHz, respectively.

In specific frequency ranges, its registered shielding effect values below - 10 dB between 6.5 to 16.88 GHz, 17.34 to 17.63 GHz (as indicated in Fig. 5). This composite material consistently maintained shielding effectiveness below - 20 dB between 6.54 and 6.98 GHz, 9.39 to 12.33 GHz, 13.33 to 13.71 GHz, 14.62 to 15.2 GHz.

In both samples the increase in the peaks at 6.6 to 8 GHz might indicate a resonant frequency where the material's structure or composition strongly interacts with the electromagnetic waves, providing enhanced shielding. The drop after 8 GHz followed by a larger peak at 16–18 GHz suggests the presence of another resonant frequency at the higher range, possibly due to higher-order modes or geometric effects of the material [43].

Chopped strands played a significant role in enhancing impedance matching and selectively targeting frequencies that contribute to the shielding efficiency of the newly developed composites at specific frequency ranges. The effectiveness of microwave shielding is closely associated with ensuring that the irradiation impedance aligns with the material's surface. The presence of the chopped strands, along with the resonance effect, has led to the emergence of distinct peaks in shielding efficiency. These chopped strands structure not only contributes to these sharp peaks but also amplifies them [44].

The interfacial polarization between chopped strands and  $\text{NiFe}_2\text{O}_4$  adds substantial value to the electromagnetic shielding composite material. The observed peaks in shielding effectiveness result from the interplay of trap geometry and the resonance effect of reflection. Furthermore, the chopped strands introduce electrical losses within the material, thereby rendering it conducive to fine-tuning the dielectric shielding effect of the  $\text{NiFe}_2\text{O}_4$  structure, consequently enhancing electromagnetic shielding effectiveness. Table 3 provides the shielding effectiveness values for epoxy-based ( $\text{NiFe}_2\text{O}_4$ / Chopped strands) composites across the GHz range.

In future research endeavors, the composite composition comprising  $\text{NiFe}_2\text{O}_4$  /Chopped strands can be subjected to more comprehensive investigations, involving the introduction of various additives or

**Table 3** Shielding effectiveness of the epoxy-(NiFe<sub>2</sub>O<sub>4</sub> / Chopped strands) composites of shielding features in GHz

Sample	SE (dB)	Frequency (GHz)
NiFe <sub>2</sub> O <sub>4</sub> / Chopped strands ( wt. % 80–20)	–36.34 –20 –10	16.56 6.5–6.92, 8.09–15.31, 15.48–16.61 6.5–16.88
NiFe <sub>2</sub> O <sub>4</sub> / Chopped strands ( wt. % 60–40)	–35.61, –33.71 –20 –10	17.51, 6.54 6.54–6.98, 9.39–12.33, 13.33–13.71, 14.62–15.20 6.5–16.88, 17.34–17.63

polymers. Exploring higher frequencies will allow for a thorough exploration of electromagnetic shielding properties, encompassing reflection loss within radar frequency bands and other frequency ranges.

## 4 Conclusions

This research thoroughly investigated the microwave shielding efficiency of NiFe<sub>2</sub>O<sub>4</sub>/Chopped strands composites, highlighting their potential as cost-effective and straightforward solutions for microwave shielding applications. The key findings from the study are as follows:

- This study established that epoxy/NiFe<sub>2</sub>O<sub>4</sub>/Chopped strands composites could serve as efficient microwave shielding materials. Their manufacturing process is both simple and cost-effective, making them suitable for widespread application.
- The X-ray diffraction (XRD) analysis confirmed that the oxide mixture method, followed by sintering at the appropriate calcination temperature, successfully produced a single-phase NiFe<sub>2</sub>O<sub>4</sub> structure with an average crystallite size of 33.2 nm. This process resulted in a homogeneous phase composition, essential for consistent material performance.
- SEM analysis revealed the exclusive presence of cubic crystalline NiFe<sub>2</sub>O<sub>4</sub> in the samples. There were no secondary phases or microstructural impurities detected, indicating a high purity level of the synthesized material.
- SEM analysis also revealed the formation of grains with diverse morphologies and defects, which significantly contribute to multiple internal reflections of electromagnetic waves. These internal reflec-

tions extend the path length of the waves within the material, thereby enhancing absorption and substantially reducing the amount of energy that passes through.

- The produced composite materials exhibited exceptional microwave shielding properties. It achieved a low shielding effectiveness of –36.34 dB at 16.56 GHz. Additionally, it maintained strong shielding effectiveness across a broad frequency range, with values below –10 dB from 6.5 to 16.88 GHz, showcasing its capacity over a wide spectrum.
- It is thought that the EM shielding feature is mostly due to magnetic spinel ferrite Ni, and the sharp shielding peaks formed are mostly due to the effect of chopped strands.
- The microwave shielding effectiveness of these composites could be further explored by incorporating various dopants. This could enhance their performance in radar and higher frequency bands. Such research could guide the development of advanced shielding and armor materials, broadening the applicability of these composites to other frequency ranges.

## Acknowledgements

This work has been edited in memorial of Salim Sahin and Emsal Sahin, Prof. Dr. Ayhan Mergen. We thank Istanbul Technical University and Adana Alparslan Türkiye Science and Technology University for their help in the investigation.

## Author contributions

Ethem İlhan Sahin: Conceptualization, Data curation, Formal analysis, Writing-original draft. Jamal-Eldin F.M. Ibrahim: Conceptualization, Data curation, Formal analysis, review & editing. Mehriban Emek: Data curation, Formal analysis, review & editing. Bahaddin Sinsoysal: Conceptualization, Formal analysis, review & editing. Alina Amanzholova: Conceptualization, Formal analysis, review & editing.

## Funding

Open access funding provided by University of Mis-kolc. The authors have not disclosed any funding.

## Data availability

Data will be made available on request.

## Declarations

**Competing interest** The authors of this work declare that they have no financial or personal interests that could have influenced their findings or conclusions.

**Open Access** This article is licensed under a Creative Commons Attribution 4.0 International License, which permits use, sharing, adaptation, distribution and reproduction in any medium or format, as long as you give appropriate credit to the original author(s) and the source, provide a link to the Creative Commons licence, and indicate if changes were made. The images or other third party material in this article are included in the article's Creative Commons licence, unless indicated otherwise in a credit line to the material. If material is not included in the article's Creative Commons licence and your intended use is not permitted by statutory regulation or exceeds the permitted use, you will need to obtain permission directly from the copyright holder. To view a copy of this licence, visit <http://creativecommons.org/licenses/by/4.0/>.

## References

1. E.İ Şahin, M. Emek, Elektromanyetik ekranlama uygulamaları için GdMnO<sub>3</sub>/PANI/Ba(Zn<sub>1</sub>/3Nb<sub>2</sub>/3)O<sub>3</sub> kompozitlerin özellikleri. *Iğdır Üniversitesi Fen Bilimleri Enstitüsü Dergisi* **13**(3), 2143–2154 (2023). <https://doi.org/10.21597/jist.1268835>
2. D. Tahir et al., Excellent electromagnetic wave absorption of Co/Fe<sub>2</sub>O<sub>3</sub> composites by additional activated carbon for tuning the optical and the magnetic properties. *J. Alloys Compd.* **864**, 158780 (2021). <https://doi.org/10.1016/j.jallcom.2021.158780>
3. V. Zaroushani, A. Khavanin, S.B. Mortazavi, A. Jnonidi, M.H. Moieni, M. Javadzadeh, The role of a new electromagnetic shielding in reducing the microwave radiation for the X-band frequencies. *Iran Occup. Health* **12**(5), 83–99 (2015)
4. E.İ Şahin, M. Emek, B. Ertug, M. Kartal, Electromagnetic shielding performances of colemanite / PANI/SiO<sub>2</sub> composites in radar and wider frequency ranges. *Beykent Üniversitesi Fen ve Mühendislik Bilimleri Dergisi* **13**(1), 34–42 (2020). <https://doi.org/10.20854/bujse.742821>
5. D.J. Panagopoulos, L.H. Margaritis, The effect of exposure duration on the biological activity of mobile telephony radiation. *Mutat. Res. Genet. Toxicol. Environ. Mutagen.* **699**(1–2), 17–22 (2010). <https://doi.org/10.1016/j.mrgentox.2010.04.010>
6. E.İ Şahin, M. Emek, Elektromanyetik kirlilik ortamında kaolinit/pva kompozitlerin elektromanyetik kalkanlama özellikleri. *Istanbul Ticaret Üniversitesi Fen Bilimleri Dergisi* **22**(43), 194–204 (2023). <https://doi.org/10.55071/ticaretfd.1252709>
7. E. İlhan Şahin Assist Mehriban Emek Jamal eldin fadoul mohammed ibrahim, *instrumental measurements laboratory*. 2023. [Online]. Available: [www.iksadyayinevi.com](http://www.iksadyayinevi.com)
8. Y. He et al., Construction of heterointerfaces and honeycomb-like structure for ultrabroad microwave absorption. *J. Colloid Interf. Sci.* **627**, 102–112 (2022). <https://doi.org/10.1016/j.jcis.2022.07.047>
9. D. Krewski, C.V. Byus, Barr, “Recent advances in research on radiofrequency fields and health.” *J. Toxicol. Environ. Health Part B* **4**(1), 145–159 (2001). <https://doi.org/10.1080/10937400121019>
10. E.İ Şahin, M. Emek, Electromagnetic shielding effectiveness of wollastonite/PANI/colemanite composites. *Avrupa Bilim ve Teknoloji Dergisi* **21**, 83–89 (2021). <https://doi.org/10.31590/ejosat.816145>
11. H. Heryanto, S. Siswanto, R. Rahmat, A. Sulieman, D.A. Bradley, D. Tahir, Nickel slag/laterite soil and nickel slag/iron sand nanocomposites: structural, optical, and electromagnetic absorption properties. *ACS Omega* **8**(21), 18591–18602 (2023). <https://doi.org/10.1021/acsomega.3c00423>
12. J. F. M. Ibrahim, A. Mergen, E. İlhan Sahin, and H. S. Basheer, “Advanced ceramics progress the effect of europium doping on the structural and magnetic properties of GdMnO<sub>3</sub> Multiferroic ceramics,” 2017.
13. L. Liu et al., Electromagnetic response of magnetic graphene hybrid fillers and their evolutionary behaviors. *J. Mater. Sci. Mater. Electron.* **27**(3), 2760–2772 (2016). <https://doi.org/10.1007/s10854-015-4088-7>
14. V. Shukla, Role of spin disorder in magnetic and EMI shielding properties of Fe<sub>3</sub>O<sub>4</sub>/C/PPy core/shell

- composites. *J. Mater. Sci.* **55**(7), 2826–2835 (2020). <https://doi.org/10.1007/s10853-019-04198-w>
15. İ Topcu, M. Ceylan, E.B. Yilmaz, Experimental investigation on mechanical properties of multi wall carbon nanotubes (Mwcnt) reinforced aluminium metal matrix composites. *J. Ceram. Process. Res.* **21**(5), 596–601 (2020). <https://doi.org/10.36410/jcpr.2020.21.5.596>
  16. İ Topcu, Investigation of wear behavior of particle reinforced AL/B4C composites under different sintering conditions. *Tehnički glasnik* **14**(1), 7–14 (2020). <https://doi.org/10.31803/tg-20200103131032>
  17. E. İ. Şahin, “Microwave electromagnetic shielding effectiveness of ZnNb<sub>2</sub>O<sub>6</sub>-chopped strands composites for radar and wideband (6.5–18 GHz) applications,” 2022.
  18. D. Cao et al., A facile strategy for synthesis of spinel ferrite nano-granules and their potential applications. *RSC Adv.* **6**(71), 66795–66802 (2016). <https://doi.org/10.1039/C6RA13373H>
  19. Z. Zhu, F. Liu, H. Zhang, J. Zhang, L. Han, Photocatalytic degradation of 4-chlorophenol over Ag/MFe<sub>2</sub>O<sub>4</sub> (M = Co, Zn, Cu, and Ni) prepared by a modified chemical co-precipitation method: a comparative study. *RSC Adv.* **5**(68), 55499–55512 (2015). <https://doi.org/10.1039/C5RA04608D>
  20. T. Tsutaoka, Frequency dispersion of complex permeability in Mn-Zn and Ni-Zn spinel ferrites and their composite materials. *J. Appl. Phys.* **93**(5), 2789–2796 (2003). <https://doi.org/10.1063/1.1542651>
  21. M. Pardavi-Horvath and M. Pardavi-Horvath, “Microwave applications of soft ferrites,” 2000. [Online]. Available: <http://www.rec-usa.com/rmhor.htm>
  22. M.A. Shayed, C. Cherif, R.D. Hund, T. Cheng, F. Osterod, Carbon and glass fibers modified by polysilazane based thermal resistant coating. *Text. Res. J.* **80**(11), 1118–1128 (2010). <https://doi.org/10.1177/0040517509357648>
  23. F.M. Zhao, N. Takeda, Effect of interfacial adhesion and statistical fiber strength on tensile strength of unidirectional glass fiber/epoxy composites. Part I: experiment results. *Compos. Part A Appl. Sci. Manuf.* **31**(11), 1203–1214 (2000). [https://doi.org/10.1016/S1359-835X\(00\)00085-3](https://doi.org/10.1016/S1359-835X(00)00085-3)
  24. A. Kumar, A.K. Singh, M. Tomar, V. Gupta, P. Kumar, K. Singh, Electromagnetic interference shielding performance of lightweight NiFe<sub>2</sub>O<sub>4</sub>/rGO nanocomposite in X- band frequency range. *Ceram. Int.* **46**(10), 15473–15481 (2020). <https://doi.org/10.1016/j.ceramint.2020.03.092>
  25. A.R. Caramitu et al., Flexible electromagnetic shielding nano-composites based on silicon and NiFe<sub>2</sub>O<sub>4</sub> powders. *Polymers (Basel)*. **15**, 11 (2023). <https://doi.org/10.3390/polym15112447>
  26. A. Radoń, Ł. Hawelek, D. Łukowiec, J. Kubacki, P. Włodarczyk, Dielectric and electromagnetic interference shielding properties of high entropy (Zn, Fe, Ni, Mg, Cd) Fe<sub>2</sub>O<sub>4</sub> ferrite. *Sci. Rep.* **9**, 1 (2019). <https://doi.org/10.1038/s41598-019-56586-6>
  27. M.F. Shakir et al., Effect of nickel-spinal-ferrites on EMI shielding properties of polystyrene/polyaniline blend. *SN Appl. Sci.* **2**, 4 (2020). <https://doi.org/10.1007/s42452-020-2535-4>
  28. H. Heryanto, D. Tahir, High absorption electromagnetic wave properties of composite cofeo<sub>3</sub> synthesized by simple mechanical alloying. *ECS J. Solid State Sci. Technol.* **10**(12), 123015 (2021). <https://doi.org/10.1149/2162-8777/ac44f4>
  29. A.F. Qasrawi, E.İ Sahin, T.Y. Abed, M. Emek, Structural and dielectric properties of Ba<sub>1-x</sub>La<sub>x</sub>(Zn<sub>1/3</sub>Nb<sub>2/3</sub>)O<sub>3</sub> solid solutions. *Phys. Status Solidi B Basic Res.* **258**, 3 (2021). <https://doi.org/10.1002/pssb.202000419>
  30. E.İ Şahin, M. Emek, J.E.F.M. Ibrahim, G. Yumuşak, M. Kartal, Shielding effectiveness performance of polyaniline-NiFe<sub>2</sub>O<sub>4</sub>: Cu composites for sub-8 GHz applications. *Opt Quantum Electron* **55**, 6 (2023). <https://doi.org/10.1007/s11082-023-04791-z>
  31. H. Heryanto, D. Tahir, Composite fayalite with 5% laterite soil and iron sand: structural properties and band gap calculation based on theoretical kubelka-munk, taylor expansion, and self-consistent field method. *JOM* **75**(12), 5264–5272 (2023). <https://doi.org/10.1007/s11837-023-05828-0>
  32. H. Heryanto, D. Tahir, Enhancing photocatalyst performance of magnetic surfaces covered by carbon clouds for textile dye degradation. *Arab. J. Sci. Eng.* (2023). <https://doi.org/10.1007/s13369-023-08532-y>
  33. P. Priyadarshini, K. Pushpanathan, Synthesis of Ce-doped NiFe<sub>2</sub>O<sub>4</sub> nanoparticles and their structural, optical, and magnetic properties. *Chem. Phys. Impact.* **1**(6), 100201 (2023). <https://doi.org/10.1016/j.chphi.2023.100201>
  34. D. D. L. Chung, “Electromagnetic interference shielding effectiveness of carbon materials,” 2001.
  35. R.S. Yadav et al., Polypropylene nanocomposite filled with spinel ferrite NiFe<sub>2</sub>O<sub>4</sub> nanoparticles and in-situ thermally-reduced graphene oxide for electromagnetic interference shielding application. *Nanomaterials* **9**, 4 (2019). <https://doi.org/10.3390/nano9040621>
  36. F. Tariq, M. Shifa, M. Tariq, S. Kazim Hasan, R.A. Baloch, Hybrid nanocomposite material for EMI shielding in spacecrafts. *Adv Mat. Res.* (2015). <https://doi.org/10.4028/www.scientific.net/amr.1101.46>
  37. E.İ Şahin, Electromagnetic shielding effectiveness of Ba(Zn<sub>1/3</sub>Nb<sub>2/3</sub>)O<sub>3</sub>: chopped strands composites for wide frequency applications. *J. Ceram. Process. Res.* **24**(1),

- 190–196 (2023). <https://doi.org/10.36410/jcpr.2023.24.1.190>
38. P. Bhardwaj, A.N. Grace, Antistatic and microwave shielding performance of polythiophene-graphene grafted 3-dimensional carbon fibre composite. *Diam. Relat. Mater.* **106**, 107871 (2020). <https://doi.org/10.1016/j.diamond.2020.107871>
39. B.P. Singh, V. Choudhary, P. Saini, R.B. Mathur, Designing of epoxy composites reinforced with carbon nanotubes grown carbon fiber fabric for improved electromagnetic interference shielding. *AIP Adv.* **2**, 2 (2012). <https://doi.org/10.1063/1.4730043>
40. B.V.S.R.N. Santhosi, K. Ramji, N.B.R.M. Rao, Design and development of polymeric nanocomposite reinforced with graphene for effective EMI shielding in X-band. *Physica B Condens Matter* **586**, 412144 (2020). <https://doi.org/10.1016/j.physb.2020.412144>
41. H. Vasquez, L. Espinoza, K. Lozano, L. Espinoza, H. Foltz, and S. Yang, “Simple device for electromagnetic interference shielding effectiveness measurement,” 2009. [Online]. Available: <https://www.researchgate.net/publication/228996699>
42. “Standard Test Method for Measuring the Electromagnetic Shielding Effectiveness of Planar Materials 1”, <https://doi.org/10.1520/D4935-10>.
43. B. Park et al., Absorption-dominant electromagnetic interference (EMI) shielding across multiple mmwave bands using conductive patterned magnetic composite and double-walled carbon nanotube film. *Adv. Funct. Mater.* (2024). <https://doi.org/10.1002/adfm.202406197>
44. H. Huang et al., Broadband radar absorbing characteristic based on periodic hollow truncated cone structure. *Phy. B Condens. Matter* (2020). <https://doi.org/10.1016/j.physb.2020.412368>

**Publisher’s Note** Springer Nature remains neutral with regard to jurisdictional claims in published maps and institutional affiliations.